ACS OMEGA

Article

Cite This: ACS Omega 2019, 4, 5915−5922

http://pubs.acs.org/journal/acsodf

Novel Colorimetric Method for Simultaneous Detection and Identification of Multimetal Ions in Water: Sensitivity, Selectivity, and Recognition Mechanism

Linfeng Chen,[†] Xike Tian,*[,†] Dasha Xia,[‡] Yulun Nie,[†] Liqiang Lu,[†] Chao Yang,[†] and Zhaoxin Zhou[†]

[†]Faculty of Materials Science and Chemistry, China University of Geosciences, Wuhan 430074, China

[‡]School of Environmental and Chemical Engineering, Jiangsu University of Science and Technology, Zhenjiang 212003, China

Supporting Information

ABSTRACT: Accurate recognition and speciation analysis of heavy-metal ions in complex hydrological environments is always a serious challenge. In this work, we proposed a small-molecule-based ultrasensitive colorimetric detection strategy and successfully applied it to the accurate detection of Fe^{2+}, Fe^{3+}, Co^{2+}, and Hg^{2+} in groundwater through the specific recognition of multiple ligands of different metal ions. The detection limits for Hg^{2+}, Co^{2+}, Fe^{2+}, and Fe^{3+} are calculated to be 6.51, 0.34, 0.49, and 1.01 ppb, respectively, which are far below the drinking water standards and superior to most of the reported colorimetric sensors. Remarkably, the speciation analysis of Fe^{2+}/Fe^{3+} also has been successfully realized by a one-step method without complex pretreatment. The speciation and concentration of Fe^{2+} and Fe^{3+} in actual water samples can be accurately identified and monitored. In addition, as an attempt of visual onsite detection, we have developed a simple test strip, which has been applied to visual monitoring of four metal ions with the detection limit estimated by the naked eye to be as low as ppb level. This proposed colorimetric method realizes the rapid, sensitive, and portable multiple metal ions recognition and Fe^{2+}/Fe^{3+} speciation analysis, displaying great potential for onsite rapid water quality analysis.

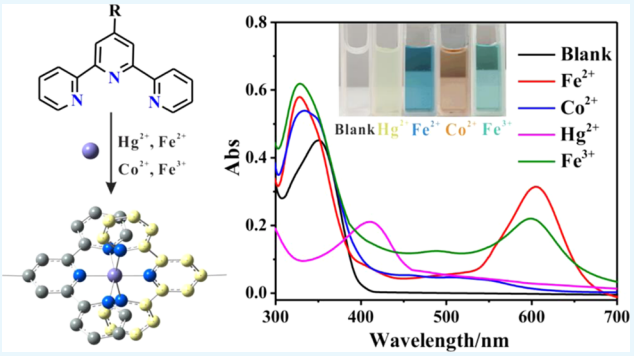

1. INTRODUCTION

Large amounts of toxic and carcinogenic heavy metal ions have been released into the environment in recent years due to the accelerated industrial and agricultural development.[1−3] The cross-contamination of heavy metals, which contains multiple or even different speciations of toxic heavy metal ions, is also increasingly common in the hydrological environments,[4,5] posing a serious threat to ecological environments and organisms.[6,7] Therefore, accurate identification and determination of heavy metal ions and their speciations are crucial. However, the complex hydrological environment makes it a big challenge to accurately detect and assess the contamination of groundwater.[8,9]

The existing analysis techniques such as atomic absorption, emission, and mass spectroscopies are based on field sampling and laboratory testing modes,[10−12] which are complicated and time consuming, and impose strict demands on the preservation and transportation of sensitive water samples. Moreover, most of the detection techniques can only realize the measurement of the total content of metal ions, whereas speciation analysis requires verbose pretreatments such as oxidation, reduction, or addition of additives.[13−16] To develop a novel detection technology for rapid, simple, and portable onsite multiple metal ions recognition and polyvalent metal speciation analysis is urgently needed. In this context, colorimetric methods have emerged as an alternative to spectroscopy-based methods because of the convenient operation, low cost, and quick responses.[17−20] The colorimetric detection of metal ions can be clearly observed by naked eyes or monitored using a portable UV−vis spectrophotometer, without resorting to cumbersome instrumental analysis.[21−23] In particular, the colorimetric probe of small molecules aroused more interest because it contains multiple recognition sites and has the potential to recognize multimetal ions simultaneously.

Herein, we proposed a small-molecule-based ultrasensitive colorimetric detection strategy and successfully realized the accurate detection of Fe^{2+}, Fe^{3+}, Co^{2+}, and Hg^{2+} in groundwater through the specific recognition of multiple ligands for different metal ions. The obtained chemosensors showed excellent stability in 100% aqueous solution and displayed different absorption spectral signals and significant color differences for four hard-to-distinguish metal ions. The detection limits for Hg^{2+}, Co^{2+}, Fe^{2+}, and Fe^{3+} are calculated

Received: February 2, 2019
Accepted: March 5, 2019
Published: March 27, 2019

DOI: 10.1021/acsomega.9b00312
ACS Omega 2019, 4, 5915−5922

Scheme 1. Synthesis Route of Tpy-QL and Tpy-BZ

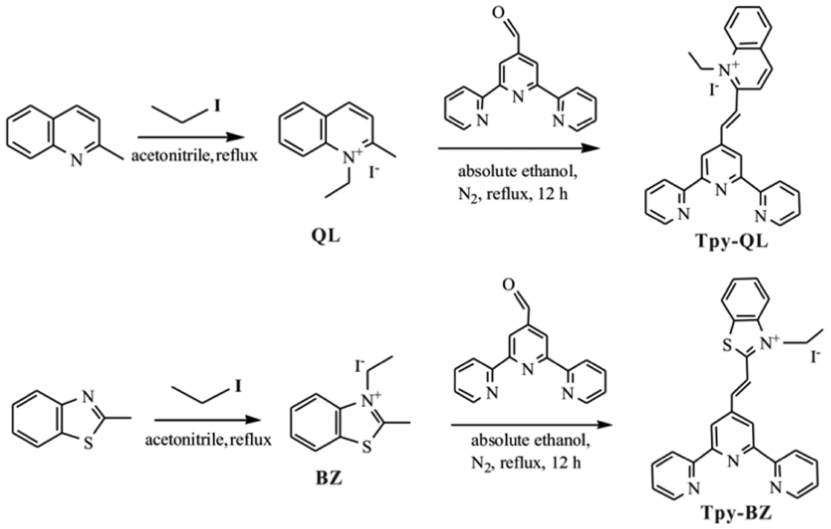

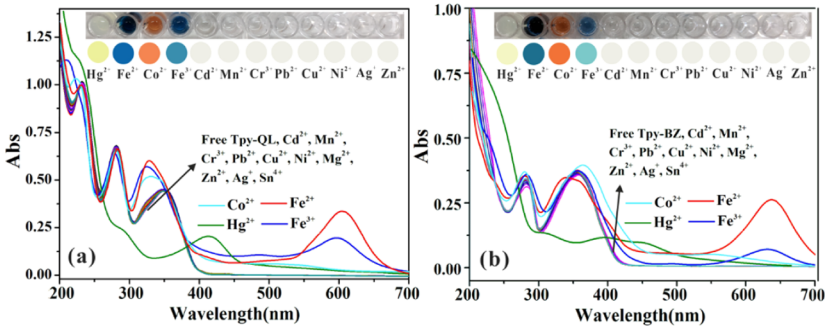

Figure 1. Absorption spectra of (a) Tpy-QL and (b) Tpy-BZ (10 μM) in 100% water solution (phosphate buffer solution (PBS) buffer, 10 mM, pH = 7.0) in the presence of different metal ions (3 equiv). Inset: (up) color patterns of the solutions using (a) Tpy-QL and (b) Tpy-BZ for different metal ions and (below) digitalized color pattern corresponding to above.

to be 6.51, 0.34, 0.49, and 1.01 ppb, respectively, which are far below the standards in drinking water recommended by World Health Organization (WHO)[24−27] and superior to most of the reported colorimetric sensors. Remarkably, the colorimetric sensors have been successfully applied to the speciation analysis of Fe^{2+}/Fe^{3+} through a one-step method without complex pretreatment, which can accurately identify and monitor the speciation and concentration of Fe^{2+} and Fe^{3+} in actual water samples. In addition, as an attempt of visual field detection, we have developed a simple test strip, which has been successfully applied to visual monitoring of four metal ions with the detection limit estimated by the naked eye to be as low as ppb level. This proposed colorimetric method realizes the rapid, sensitive, and portable multiple metal ions recognition and Fe^{2+}/Fe^{3+} speciation analysis, displaying great potential for onsite rapid water quality analysis.

2. RESULTS AND DISCUSSION

2.1. Synthesis of Tpy-QL and Tpy-BZ. Efficient detection of multiple metal ions means that efficient ligands are required. Terpyridine (Tpy) is considered as a good candidate because it contains three strongly chelating N elements. In addition, terpyridine possesses a typical conjugated system that has great potential to cause fluorescence or absorption spectrum changes and even induce significant color changes when coupling with metal ions, which is of great significance for visual monitoring. However, the unsatisfactory water solubility limits its further application. We herein introduce hydrophilic groups quinolinium iodide (QL) and benzothiazolium iodide (BZ) to terpyridine backbone to improve hydrophilicity. The synthesize procedures of terpyridine derivatives Tpy-QL and Tpy-BZ are outlined in Scheme 1. All products were purified by column chromatography and then characterized by NMR and high-resolution mass spectrum (HRMS), from which satisfactory data were obtained corresponding to their molecular structures.

2.2. Colorimetric Detection of Multimetal Ions. As expected, the introduction of quinolinium iodide and benzothiazolium iodide endow Tpy-QL and Tpy-BZ with excellent hydrophilicity, which means that they can be completely dissolved in 100% aqueous solution. Subsequently, we carefully investigated the binding ability of Tpy-QL and Tpy-BZ toward different metal ions by UV−vis spectra in water solution. As shown in Figure 1, the free Tpy-QL and Tpy-BZ in water displayed two characteristic absorption bands at 282 and 354 nm and 280 and 360 nm, which were assignable to $\pi \rightarrow \pi^*$ intramolecular charge-transfer transitions. This absorption spectrum was almost unchanged when 5 equiv of metal ions (Cd^{2+}, Mn^{2+}, Cr^{3+}, Pb^{2+}, Cu^{2+}, Ni^{2+}, Mg^{2+}, Zn^{2+}, Ag^{+}) were added. However, remarkable spectrum changes along with distinct color transformation could be observed upon the addition of Hg^{2+}, Co^{2+}, Fe^{2+}, or Fe^{3+}. Moreover, the spectral changes caused by these four

DOI: 10.1021/acsomega.9b00312
ACS Omega 2019, 4, 5915−5922

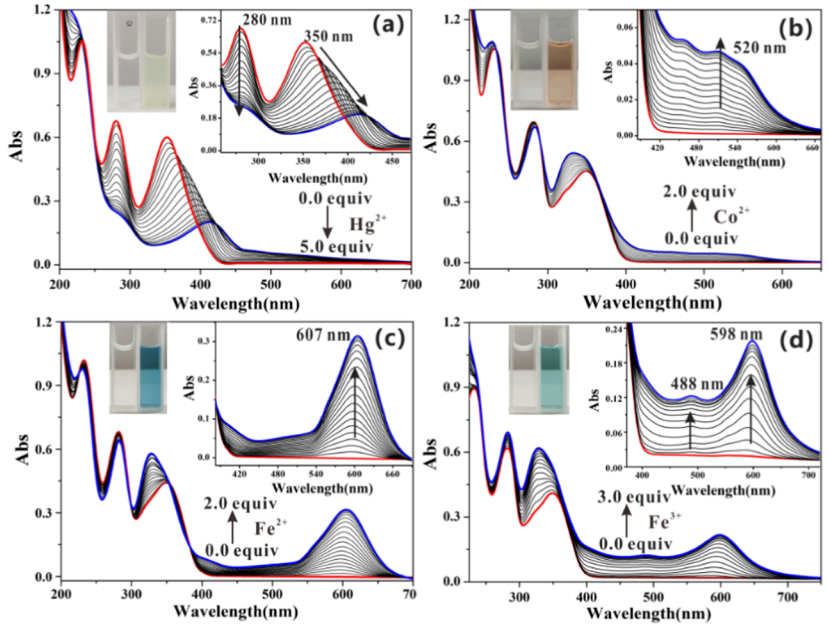

Figure 2. UV−vis titrations spectra of Tpy-QL (10 μM) in water (PBS buffer, 10 mM, pH = 7.0) in the presence of various concentrations of (a) Hg^{2+}, (b) Co^{2+}, (c) Fe^{2+}, and (d) Fe^{3+}. The red line represents the spectrum of free Tpy-QL in water and blue line represents the spectrum after reaction saturation. The inset photographs were taken after the Tpy-QL and metal ions were completely reacted.

metal ions were completely different, so were the color changes.

Next, we focused on the changes in absorption spectra of Hg^{2+}, Co^{2+}, Fe^{2+}, and Fe^{3+} after binding to Tpy-BZ and Tpy-QL. As depicted in Figure 2a, the bands at 282 and 354 nm gradually decreased and finally the band at 282 nm vanished with the addition of Hg^{2+}. Meanwhile, the decrease of band at 354 nm was accompanied by a significant red shift from 354 to 409 nm. Accordingly, an obvious color change from colorless to pale yellow was observed. For the titration of Co^{2+}, the band at 282 nm was almost unchanged and the band at 354 nm was slightly enhanced, whereas a new band at 520 nm formed and developed, which led to significant color change from colorless to pink. Unlike Co^{2+}, this newly emerging absorption band was transferred to 607 nm when Fe^{2+} ions were added and sharply enhanced as the concentration of Fe^{2+} increased. Furthermore, the color quickly turned into blue. Interestingly, when Fe^{3+} was introduced into Tpy-QL solution, the phenomenon was also different from that of Fe^{2+}. As shown in Figure 2d, in the presence of Fe^{3+}, the band at 607 nm was slightly blue-shifted to 598 nm and the intensity was reduced to half. Meanwhile, an inconspicuous band gradually appeared at 488 nm as the Fe^{3+} concentration increased. Undoubtedly, such a phenomenon that one chemosensor exhibits completely different spectral change and colors than multiple metal ions is extremely rare, which can be used for colorimetric detection of multiple metal ions. Moreover, similar results that exhibited completely different absorption bands and color changes for Hg^{2+}, Co^{2+}, Fe^{2+}, and Fe^{3+} could be observed when investigating Tpy-BZ (Figure S1). We also carefully studied the stability of Tpy-QL and Tpy-BZ after the addition of excess metal ion. As shown in Figure S2, the absorption intensities of Tpy-QL and Tpy-BZ were quite stable and almost no changes were observed within 150 min. This result indicated that Tpy-QL and Tpy-BZ had good stability in aqueous solution and met the detection requirements.

To assess the sensitivity, different concentrations of Hg^{2+}, Co^{2+}, Fe^{2+}, and Fe^{3+} were added to the Tpy-QL solution (10 μM). As shown in Figure S3, good linear relationships between the absorbance intensity and the specified concentration range were obtained. The corresponding detection limits (LOD = $3\sigma/s$) were also calculated to be 32.56 nM (Hg^{2+}), 5.89 nM (Co^{2+}), 8.75 nM (Fe^{2+}), and 17.89 nM (Fe^{3+}), which were much lower than the majority of the reported colorimetric sensor (Tables S1−S4). The detection performance of Tpy-BZ was also analyzed (Figure S4), and the detection limits calculated by the same method were 27.69 nM (Hg^{2+}), 4.81 nM (Co^{2+}), 5.58 nM (Fe^{2+}), and 24.73 nM (Fe^{3+}), which were basically consistent with that for Tpy-QL. Such low detection limits and distinct color changes promise their practical application for detecting Hg^{2+}, Co^{2+}, Fe^{2+}, and Fe^{3+} in water.

The colorimetric sensors not only exhibited excellent sensitivity to Hg^{2+}, Co^{2+}, Fe^{2+}, and Fe^{3+} but also displayed good selectivity. Take Tpy-QL as an example, as shown in Figure 3, it only showed distinct differential absorption signal for Hg^{2+}, Co^{2+}, Fe^{2+}, and Fe^{3+} but no change for other metal ions, showing good selectivity. The interference tests were subsequently operated by adding corresponding ions to the probe solution containing the interference cations. The results indicated that signal recovery of Hg^{2+}, Co^{2+}, Fe^{2+}, or Fe^{3+} was not affected by the coexisting metal ions or anions.

The Job's plot analysis was executed to investigate the reaction ratio between sensors and metal ions. The measured absorbance intensity reached a maximum when the molar fraction of ($[M^{n+}]/[[M^{n+}] + [\text{Tpy-QL}]]$) was approximately 0.33, suggesting that Tpy-QL reacted with Hg^{2+}, Co^{2+}, Fe^{2+}, and Fe^{3+} in 2:1 stoichiometry (Figure S5). Further, the binding affinity of Tpy-QL and Tpy-BZ for Hg^{2+}, Co^{2+}, Fe^{2+}, and Fe^{3+} was estimated from the Benesi−Hildebrand[28] plots. By using the linear fitting of absorbance titration data with 1:2 binding model (Figure S6), the association constants (K_a) of Tpy-QL for four metal ions were estimated to be 2.89×10^2 $M^{-1/2}$ (Hg^{2+}), 3.12×10^2 $M^{-1/2}$ (Co^{2+}), 3.31×10^2 $M^{-1/2}$ (Fe^{2+}), and

DOI: 10.1021/acsomega.9b00312
ACS Omega 2019, 4, 5915−5922

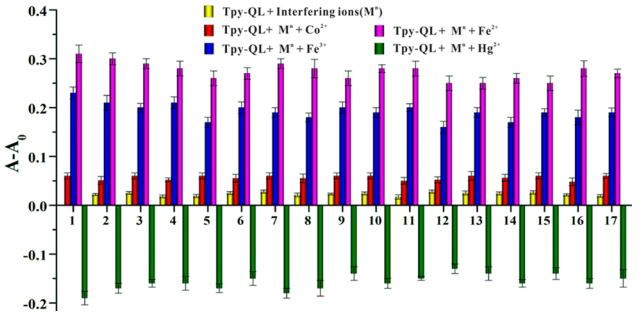

Figure 3. Selectivity and interference testing of Tpy-QL (10 μM) for common metal ions and anions in water (PBS buffer, 10 mM, pH = 7.0). A_0 is the absorbance intensity of free Tpy-QL, A is the absorbance intensity after the addition of metal ions (collected at 520 nm for Co^{2+}, 280 nm for Hg^{2+}, 607 nm for Fe^{2+}, and 598 nm for Fe^{3+}). (1) Represent the $A - A_0$ of Tpy-QL for Co^{2+}, Fe^{3+}, Fe^{2+}, and Hg^{2+} and (2−17) represent Cd^{2+}, Mn^{2+}, Cr^{3+}, Pb^{2+}, Cu^{2+}, Ni^{2+}, Mg^{2+}, Zn^{2+}, Ag^{+}, Sn^{4+}, HPO_4^{2-}, $H_2PO_4^{-}$, HSO_3^{-}, ClO^{-}, CH_3COO^{-}, SO_3^{2-}, and HCO_3^{-}.

3.70×10^2 $M^{-1/2}$ (Fe^{3+}). Using the same method, the K_a of Tpy-BZ for four metal ions were estimated to be 2.71×10^2 $M^{-1/2}$ (Hg^{2+}), 3.03×10^2 $M^{-1/2}$ (Co^{2+}), 3.05×10^2 $M^{-1/2}$ (Fe^{2+}), and 3.26×10^2 $M^{-1/2}$ (Fe^{3+}). Obviously, there is no significant difference in the binding ability of Tpy-BZ and Tpy-QL to four metal ions.

2.3. Speciation Analysis of Fe^{2+}/Fe^{3+}. In view of the critical role of different speciation of iron ions in the redox process in environmental systems, accurate detection of iron ions with different oxidation states and corresponding concentrations is of great significance. However, methods for simultaneously detecting Fe^{2+} and Fe^{3+} in samples are rarely reported and only total concentration or specific oxidation state for iron ions can be measured. Here, both Tpy-BZ and Tpy-QL exhibit different absorption signals for Fe^{2+} and Fe^{3+}, demonstrating the potential for simultaneous identification and detection of Fe^{2+} and Fe^{3+}. Figure 4a shows the absorption spectra of Tpy-QL for different molar ratios of Fe^{2+}/Fe^{3+}. With the increase of Fe^{3+} molar ratio, the characteristic absorption band of Fe^{3+} at 488 nm was gradually enhanced, whereas the absorption band of Fe^{2+} at 607 nm was gradually weakened and blue-shifted to 598 nm. By calculating the absorption peak area at 488 nm (S_{488}) and 598 nm (S_{598}) (Figure S7), we found that the peak area sum of $S_{598} + S_{488}$ was a constant value at a specific total iron concentration and was not affected by the ratio of Fe^{2+} (Figure 4b). Interestingly, $S_{598} + S_{488}$ was proportional to the total iron concentration and showed a good linear relationship in the concentration range of 0−8 μM (Figure 5a). Moreover, the ratio of peak area (S_{598}/S_{488}) was closely related to the molar ratio of Fe^{2+}, with a correlation coefficient of 0.998 (Figure 5b). Therefore, the total Fe concentration can be quantitatively analyzed using $S_{598} + S_{488}$, and the molar ratio of Fe^{2+} and Fe^{3+} can be ascertained by S_{598}/S_{488}, thus realizing the speciation analysis of Fe^{2+}/Fe^{3+}.

2.4. Mechanism Studies. We monitored the reactions of Tpy-QL and Tpy-BZ with metal ions by ^{1}H NMR titration experiments in DMSO-d_6. However, we failed to obtain the ^{1}H NMR spectra of Tpy-QL-Fe^{2+}, Tpy-QL-Fe^{3+}, and Tpy-QL-Co^{2+} due to the strong interference of lone electron in Fe^{2+}, Fe^{3+}, and Co^{2+} compounds, and only the ^{1}H NMR spectra of Tpy-QL-Hg^{2+} was available. As shown in Figure 6, all pyridine protons on Tpy-CHO, Tpy-BZ, and Tpy-QL exhibited varying degrees of up-shift after reaction with 5 equiv of Hg^{2+}, whereas the aldehyde proton or quinoline ring protons remained unchanged. This result indicated the electron density on the pyridine rings was reduced after reaction, implying all pyridine rings were involved in the reaction and the electrons may flow to the metal moiety.

To get a deep insight into the binding mode, the geometry optimizations and electronic calculations for several possible complex structures of Tpy-QL and metal ions with a 2:1 stoichiometry were performed using the B3LYP functional and Gaussian 09 package. The calculated optimized structures indicated that the binding sites of Tpy-QL with metal ions were the pyridine nitrogen. As depicted in Figure 7a, each Hg^{2+} ion chelated with six pyridine nitrogen of two Tpy-QL molecules to form a stable six-coordinate structure. The two Tpy-QL molecules were almost perpendicular to each other, with an angle of 91.28°, the length of the Hg−N bonds was 1.97 Å, and the angle of the coordinate bond was 81.55°. Similar calculated results could be obtained from Tpy-QL-Fe^{2+}, Tpy-QL-Fe^{3+}, and Tpy-QL-Co^{2+} (Figure S8), and the structural parameters were all within the reasonable range of stable structures (Table S5). These results implied the difference in absorption spectra root in diverse chemical properties of the metal ions, rather than the differences in the chelating mode.

The electron transformations of Tpy-QL before and after reaction with Hg^{2+}, Co^{2+}, Fe^{2+}, and Fe^{3+} were investigated using Multiwfn package. As displayed in Figure 7b, the blue region indicated a decrease in electron density after the reaction, meaning that electrons were contributed. The purple area indicated an increase in electron density, implying an

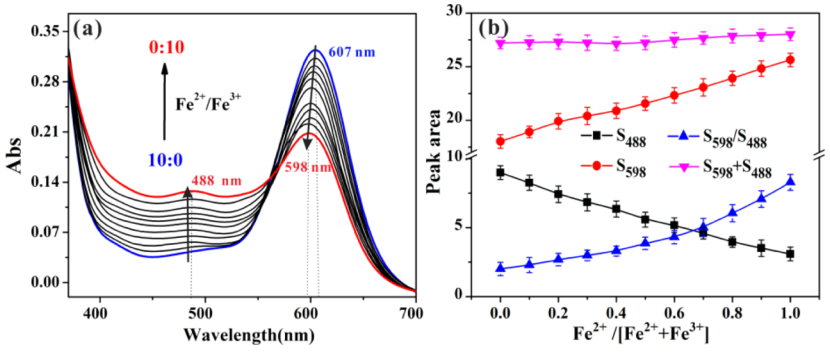

Figure 4. (a) Absorbance spectra of Tpy-QL (10 μM) upon changing the mole ratio of Fe^{2+}/Fe^{3+} ([Fe^{2+}] + [Fe^{3+}] = 10 μM). (b) Relationship between the peak area (S_{598}, S_{488}, $S_{598} + S_{488}$, S_{598}/S_{488}) and the percentage of Fe^{2+}.

DOI: 10.1021/acsomega.9b00312
ACS Omega 2019, 4, 5915−5922

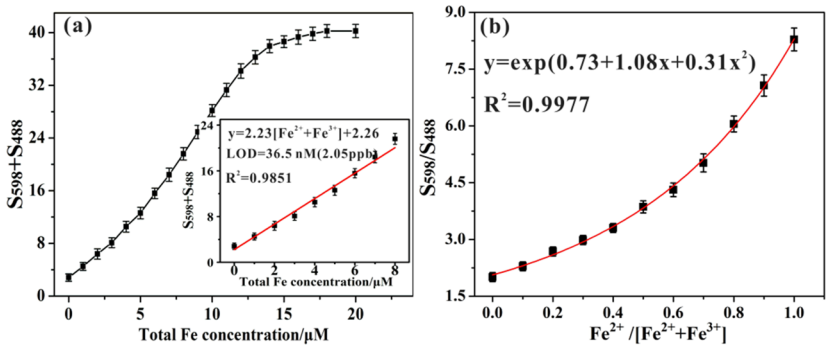

Figure 5. (a) Plot of $S_{598} + S_{488}$ vs the total iron concentrations ([Fe^{2+}] + [Fe^{3+}]). Inset: linear fitting curve of $S_{598} + S_{488}$ with respect to the total iron concentrations in the range of 0−8 μM. (b) Plot of peak area ratio S_{598}/S_{488} as a function of the Fe^{2+} percentage content.

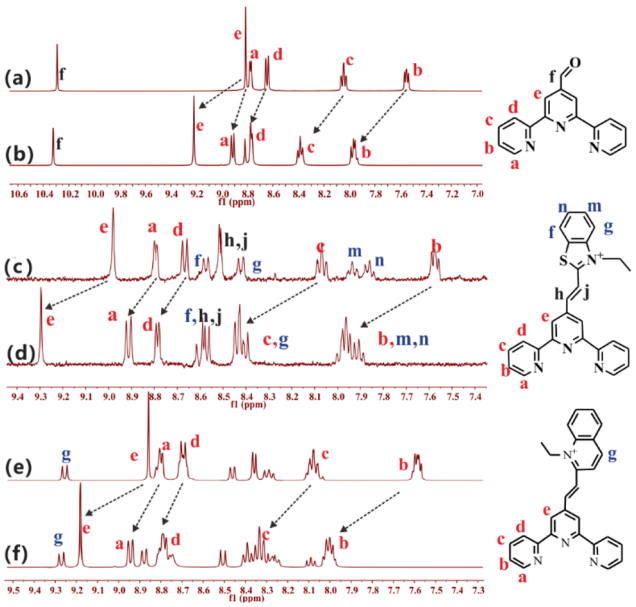

Figure 6. ^{1}H NMR spectra of Tpy-CHO, Tpy-BZ, and Tpy-QL in DMSO-d_6 before (a, c, e) and after (b, d, f) the addition of 5 equiv of Hg^{2+}.

inflow of electrons. Obviously, the electrons on the pyridine ring, especially on the N atom, significantly flowed to the metal center during the reaction, whereas the electron density on the quinoline moiety was almost unchanged, being highly consistent with the ^{1}H NMR experimental phenomenon. In addition, the two-dimensional electron density color-filled maps of Tpy-QL-Hg^{2+} could provide more evidence that the electron density of terpyridine moiety decreased significantly after binding to mercury ions (Figure 8).

2.5. Analytical Applications in Real Water Samples.

Considering the excellent stability, selectivity, and sensitivity of Tpy-QL and Tpy-BZ to Hg^{2+}, Co^{2+}, Fe^{2+}, and Fe^{3+}, their detection performances in the natural water samples are expected. Herein, the analysis of natural water samples and standard addition recovery experiments were carried out to verify the practicability of the proposed method. As depicted in Table 1, the found values of four metal ions were consistent with the spiked values and agreed with the inductively coupled plasma-optical emission spectroscopy (ICP-AES) results, demonstrating the validity of the sensors to the natural water samples. Next, we carefully investigated the feasibility of the sensors for the speciation analysis of Fe^{2+}/Fe^{3+} by adding different molar ratios of Fe^{2+} and Fe^{3+} (total concentration was 100 ppb) into different natural water samples. As shown in Table 2, the found values were all consistent with the added values in tap water, Yangtze River water, and Jianghan Plain groundwater samples. The sum of Fe^{2+} and Fe^{3+} concentrations measured by the proposed colorimetric method was in good agreement with the ICP-AES results, and the standard deviation was within the error tolerance. This result showed that the presented method had the ability to simultaneously recognize Fe^{2+} and Fe^{3+} in Fe^{2+}/Fe^{3+} mixtures, displaying the potential for speciation analysis of Fe^{2+}/Fe^{3+} in actual samples.

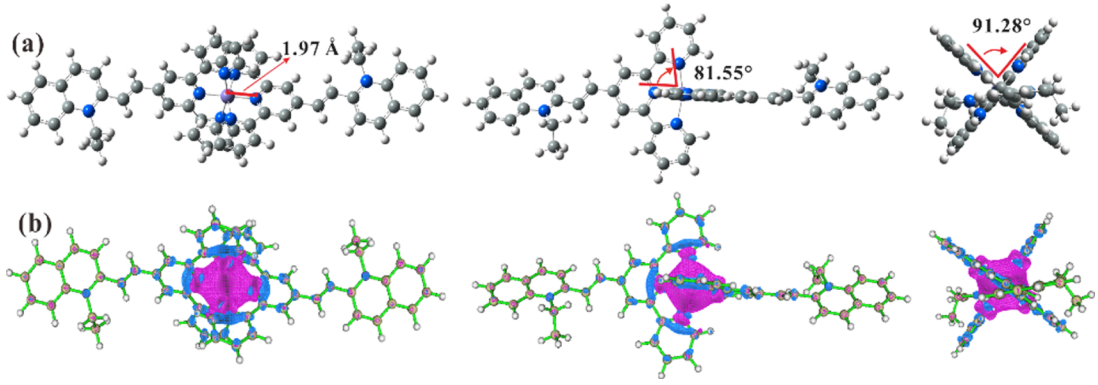

Figure 7. (a) Different observation view of density functional theory (DFT) calculated optimization Tpy-QL-Hg^{2+} structure. (b) Corresponding electron density changes before and after the reaction of Tpy-QL with Hg^{2+}. The blue area indicates decrease in electron density after the reaction, whereas the purple area indicates increase in electron density.

DOI: 10.1021/acsomega.9b00312
ACS Omega 2019, 4, 5915−5922

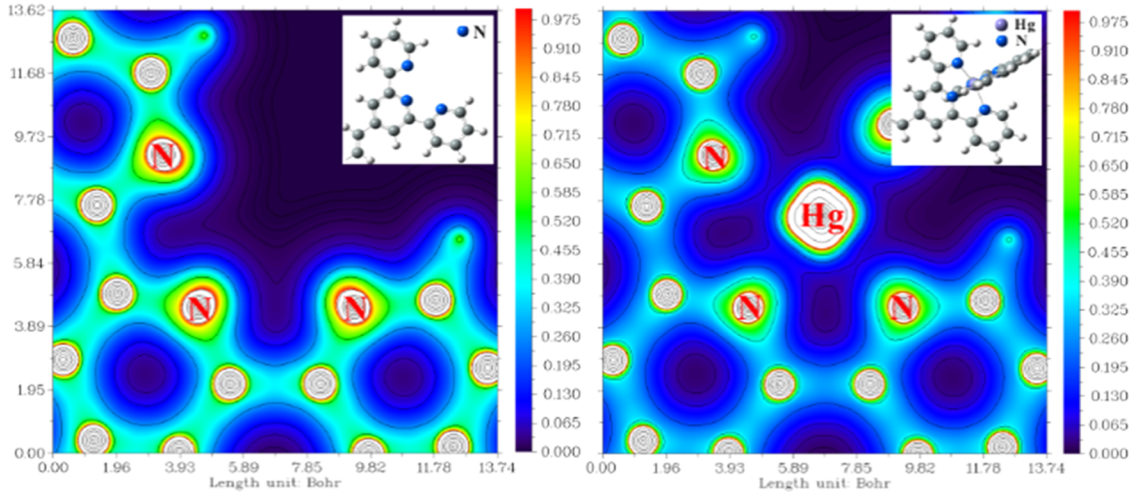

Figure 8. Two-dimensional electron density color-filled maps of partial Tpy-QL (left) and Tpy-QL-Hg^{2+} (right). Inset: corresponding DFT-calculated optimum partial structure.

Table 1. Detection of Hg^{2+}, Co^{2+}, Fe^{2+}, and Fe^{3+} in Natural Water Samples after Adding Standard Concentration of the Corresponding Metal Ions

		Hg^{2+}[a]			Co^{2+}[a]			Fe^{2+}[a]			Fe^{3+}[a]		
samples	spiked/ppb	found/ppb	RDS%	ICP-AES	found/ppb	RDS%	ICP-AES	found/ppb	RDS%	ICP-AES	found/ppb	RDS%	ICP-AES
tap water	blank	[b]											
	30.0	26.5	6.4	31.9	28.5	4.8	32.1	31.5	4.6	27.8	28.9	6.1	26.7
	100.0	97.4	3.1	104.3	97.6	2.9	92.4	97.3	3.1	94.5	92.1	2.9	109.2
	300.0	317.4	2.9	302.6	291.3	1.7	278.3	292.0	2.0	278.3	311.2	1.8	284.4
Yangtze River water	blank			1.8	0.9	10.7		0.8	11.5	2.5[c]			2.5[c]
	30.0	25.4	7.1	29.1	27.9	5.1	25.9	32.1	3.8	32.7	31.3	8.3	27.9
	100.0	101.2	3.2	105.4	98.4	2.7	91.3	102.5	1.7	105.5	111.2	3.2	102.6
	300.0	329.9	1.9	305.6	287.5	2.2	264.7	314.0	1.3	308.7	317.4	2.7	315.4
Jianghan Plain groundwater	blank			2.6	1.4	9.4	2.3	1.6	9.1	3.7[c]			3.7[c]
	30.0	25.7	7.5	36.5	32.2	2.5	31.0	27.4	3.5	32.4	31.2	7.4	31.9
	100.0	104.5	3.7	110.2	104.3	1.6	97.5	110.1	1.4	106.5	98.7	2.3	107.6
	300.0	335.8	2.6	308.7	291.4	1.0	271.6	325.6	0.9	319.4	308.9	2.0	322.2

[a]Average of three measurements. [b]Below the detection limit. [c]Specified speciation cannot be measured and the values are the total iron concentration.

Table 2. Speciation Analysis of Fe^{2+}/Fe^{3+} in Natural Water Samples

	added (100 ppb)	found/ppb[a]		
sample	Fe^{2+}/Fe^{3+} (ppb)	Fe^{2+}	Fe^{3+}	ICP-AES/ppb[a]
tap water	blank	[b]		
	20/80	18.42 ± 0.88	83.17 ± 0.27	105.23 ± 0.23
	50/50	47.38 ± 0.42	48.68 ± 0.32	97.18 ± 0.19
	80/20	76.91 ± 0.47	19.23 ± 1.04	95.95 ± 0.51
Yangtze River water	blank	1.42 ± 0.26		2.54 ± 0.34
	20/80	17.25 ± 1.12	81.55 ± 0.29	101.35 ± 0.45
	50/50	51.06 ± 0.50	54.64 ± 0.43	106.23 ± 0.36
	80/20	77.28 ± 0.21	21.27 ± 0.79	97.91 ± 0.57
Jianghan Plain groundwater	blank	2.04 ± 0.33	1.51 ± 0.24	3.69 ± 0.27
	20/80	16.39 ± 0.86	88.06 ± 0.62	98.37 ± 0.42
	50/50	47.71 ± 0.51	52.38 ± 0.56	102.39 ± 0.28
	80/20	82.13 ± 0.33	18.29 ± 0.84	105.37 ± 0.31

[a]Average of three measurements + standard deviation. [b]Below the detection limit.

Onsite visual monitoring is of great significance for water quality analysis. Here, as an attempt, we developed a simple test strip for visual detection of metal ions by immersing ordinary filter paper into the water mixtures of poly(vinyl alcohol) and Tpy-QL. As shown in Figure 9, the test strips displayed different colors for Hg^{2+}, Co^{2+}, Fe^{2+}, and Fe^{3+}, and the color deepened as the concentration increases. It should be noted that this test strip is very stable and can be stable for at least 2 weeks. The detection limits observed by the naked eye were estimated to be 10, 25, 10, and 200 ppb for Fe^{2+}, Fe^{3+},

DOI: 10.1021/acsomega.9b00312
ACS Omega 2019, 4, 5915−5922

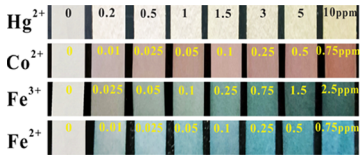

Figure 9. Photographs of the test strips of Tpy-QL for the visual detection of Hg^{2+}, Co^{2+}, Fe^{2+}, and Fe^{3+}.

Co^{2+}, and Hg^{2+}, respectively, which were attractive for onsite visual inspection. However, we should be soberly aware that this strip still has a long way to go before it can be accurately applied to complex actual samples.

3. CONCLUSIONS

In summary, we have successfully developed two small-molecule-based ultrasensitive colorimetric method for Fe^{2+}, Fe^{3+}, Co^{2+}, and Hg^{2+} detection in groundwater. Tpy-QL and Tpy-BZ had the ability to specifically chelate with Fe^{2+}, Fe^{3+}, Co^{2+}, and Hg^{2+} with a stoichiometric ratio of 2:1, exhibiting different absorption responses and color changes. The detection limits for Hg^{2+}, Co^{2+}, Fe^{2+}, and Fe^{3+} were calculated to be 6.51, 0.34, 0.49, and 1.01 ppb, respectively, which were superior to that of most of the reported chemosensors. Moreover, the sensors have been successfully applied to speciation analysis of Fe^{2+}/Fe^{3+}. The recovery test of the actual water sample indicated that the measurement results by sensors were well consistent with the added values and matched with the ICP-AES results, demonstrating the feasibility of the proposed method for multitarget recognition and speciation analysis. In addition, as an attempt of visual field detection, the simple test strips have been successfully developed and applied to visual monitoring of four metal ions with the detection limit estimated by the naked eye to be as low as ppb level.

4. MATERIALS AND METHODS

4.1. Reagents and Instruments. 2-Melthylchinolin, 2-methyl-benzothiazol, and poly(vinyl alcohol) (PVA) were purchased from Sinopharm Chemical Reagent Co., Ltd. Tripyridine-4-carbaldehyde were obtained from Alpha Chemical Co. Ltd. All reagents were used directly without purification. All the aqueous solutions used in this experiment were ultrapure water with a resistivity of 18.25 MΩ cm. Metal ion solution was preferably prepared using chloride, followed by nitrate. Ferrous-ion solution was unstable in aqueous solution and must be used immediately after preparation.

The structure of obtained organic products was characterized by HRMS (GCT premier CAB048 mass spectrometer) and ^{1}H NMR (Bruker Avance 400 MHz NMR spectrometer). The absorbance spectra of Tpy-QL and Tpy-BZ were collected from Perkin Elmer Lambda 35 spectrophotometer.

4.2. Synthesis of Terpyridyl-Based Colorimetric Sensors. The Tpy-BZ was prepared according to the procedures provided in the literature.[29] 2-Methylbenzothiazole was first ethylated to hydrophilic benzothiazolium iodide. Briefly, 150 mg (1 mmol) of 2-methyl-benzothiazol and 156 mg (1 mmol) of iodoethane were added into 20 mL of acetonitrile and then refluxed for 6 h. After reaction, 150 mL of diethyl ether was introduced to precipitate the solid and then the desired *N*-ethyl-2-methyl-benzothiazolium iodide salt was collected by filtration under reduced pressure and washed several times with diethyl ether. For the synthesis of Tpy-BZ, 0.2 mmol of obtained iodide salt and 0.2 mmol of tripyridine-4-carbaldehyde were condensed in 5 mL of absolute ethanol at reflux for 12 h in the dark under N_2 atmosphere. After reaction, the mixtures were concentrated under reduced pressure and purified by silica gel column chromatography to get faint yellow Tpy-BZ (66.8 mg, yield 61%). Tpy-QL was obtained by a similar synthetic procedure with a yield of 56% (60.7 mg). The characterization data are provided in Figures S9−S16.

4.3. Spectral Measurements. The stock solution of probes and metal ions were prepared in 100% water solution with the concentration of 0.2 mM. For Fe^{2+}, Fe^{3+}, Co^{2+}, and Hg^{2+} detection, 50 μL of probe solution was first added into the quartz cuvette, followed by 50 μL of PBS buffer solution (pH = 7.0, 10 mM) and 1.9 mL of water. Then, different volumes of metal ions stock solution (0.2 mM) were successively added into the sensor solution, the absorbance signal was collected 30 s after each addition. The responses of probe for other metal ions were carried out using the same procedure.

4.4. Application in Natural Water Samples. The detection effect of the proposed colorimetric method for Fe^{2+}, Fe^{3+}, Co^{2+}, and Hg^{2+} were carefully investigated in natural water by spiked different amounts of standard sample. The natural water samples were collected from tap water, Yangtze River water, and Jianghan Plain groundwater. The obtained samples were first filtered to remove solid impurities and then neutralized with PBS buffer solvent (pH = 7.0). For analysis, the blank natural water samples were first analyzed by the proposed colorimetric method. Then, different amounts of Fe^{2+}, Fe^{3+}, Co^{2+}, and Hg^{2+} were added into three natural water samples, making the metal ion concentration in the water samples to be 30, 100, and 300 ppb, respectively. The prepared samples were tested immediately at room temperature using the proposed colorimetric method, and each concentration was done in triplicate. The obtained results were compared with the ICP-AES results.

The speciation analysis of Fe^{2+}/Fe^{3+} was operated in natural water samples. For analysis, different concentrations of Fe^{2+} and Fe^{3+} (20/80, 50/50, 80/20 ppb) were first added to the actual water samples, the total concentration of Fe^{2+} + Fe^{3+} was kept at 100 ppb, and then tested by the proposed method. Each concentration was measured in triplicate and verified by ICP-AES.

4.5. Preparation of Test Strips for Visual Detection. The test strips for Fe^{2+}, Fe^{3+}, Co^{2+}, and Hg^{2+} were prepared based on the reported method with minor modifications.[30] One gram of PVA was first introduced into 20 mL of water and then stirred vigorously under heating until completely dissolved. After cooling to room temperature, 1 mL of Tpy-QL water solution (5 mM) was added into 5 mL of PVA solution and stirred until it a clear solution was obtained. Finally, the mixtures of Tpy-QL and PVA were evenly smeared on the surface of the common filter paper and dried at room temperature. For the visual detection of metal ions, different concentrations of Fe^{2+}, Fe^{3+}, Co^{2+}, and Hg^{2+} were prepared in 10 mL beaker and then the obtained strips were immersed in different metal ion solutions for 30 seconds.

4.6. Theoretical Calculation. All of the theoretical calculations were carried out using the Gaussian 09 package.[31] The C, N, and H atoms were described by the hybrid exchange−correlation functional B3LYP. 6-31G* basis sets, and the metal atoms were described by Lanl2dz basis sets. All

DOI: 10.1021/acsomega.9b00312
ACS Omega 2019, 4, 5915−5922

of the electron density analyses were performed using the Multiwfn package.[32]

■ ASSOCIATED CONTENT

Supporting Information

The Supporting Information is available free of charge on the ACS Publications website at DOI: 10.1021/acsomega.9b00312.

Titrations spectra of Tpy-BZ, Job's plot, Benesi–Hildebrand plot, detection limits, DFT calculation, structural parameters of theoretical calculation, ^{1}H NMR, and HRMS characterizations (PDF)

■ AUTHOR INFORMATION

Corresponding Author

*E-mail: xktian@cug.edu.cn.

ORCID

Xike Tian: 0000-0001-9406-5291

Notes

The authors declare no competing financial interest.

■ ACKNOWLEDGMENTS

This work was supported by the National Natural Science Foundation of China (Nos. 41807200, 41773126, and 51878633) and the Foundation for Innovative Research Groups of the National Natural Science Foundation of China (No. 41521001) and the "Fundamental Research Funds for the Central Universities".

■ REFERENCES

(1) Srivastava, S.; Agrawal, S. B.; Mondal, M. K. A review on progress of heavy metal removal using adsorbents of microbial and plant origin. *Environ. Sci. Pollut. Res.* **2015**, *22*, 15386–15415.

(2) Tchounwou, P. B.; Ayensu, W. K.; Ninashvili, N.; Sutton, D. Review: Environmental exposure to mercury and its toxicopathologic implications for public health. *Environ. Toxicol.* **2003**, *18*, 149–175.

(3) Sud, D.; Mahajan, G.; Kaur, M. P. Agricultural waste material as potential adsorbent for sequestering heavy metal ions from aqueous solutions - a review. *Bioresour. Technol.* **2008**, *99*, 6017–6027.

(4) Khan, S.; Cao, Q.; Zheng, Y. M.; Huang, Y. Z.; Zhu, Y. G. Health risks of heavy metals in contaminated soils and food crops irrigated with wastewater in Beijing, China. *Environ. Pollut.* **2008**, *152*, 686–692.

(5) Taylor, S. R.; Mclennan, S. M. The geochemical evolution of the continental crust. *Rev. Geophys.* **1995**, *33*, 241–265.

(6) Wang, J.; Chen, C. Biosorbents for heavy metals removal and their future. *Biotechnol. Adv.* **2009**, *27*, 195–226.

(7) Antonovics, J.; Bradshaw, A. D.; Turner, R. G. Heavy Metal Tolerance in Plants. *Adv. Ecol. Res.* **1971**, *7*, 1–85.

(8) Diels, L.; Lelie, N. V. D.; Bastiaens, L. New developments in treatment of heavy metal contaminated soils. *Environ. Sci. Biotechnol.* **2002**, *1*, 75–82.

(9) Chen, L.; Tian, X.; Zhao, Y.; Li, Y.; Yang, C.; Zhou, Z.; Liu, X. A ratiometric fluorescence nanosensor for highly selective and sensitive detection of selenite. *Analyst* **2016**, *141*, 4685.

(10) Zeini, J. E.; Bidari, A.; Assadi, Y.; Milani Hosseini, M. R.; Jamali, M. R. Dispersive liquid-liquid microextraction combined with graphite furnace atomic absorption spectrometry: ultra trace determination of cadmium in water samples. *Anal. Chim. Acta* **2007**, *585*, 305–311.

(11) Hatch, W. R.; Ott, W. L. Determination of submicrogram quantities of mercury by atomic absorption spectrophotometry. *Anal. Chem.* **1968**, *40*, 2085.

(12) Beauchemin, D. Inductively coupled plasma mass spectrometry handbook, Simon M. Nelms, Editor, Blackwell Publishing Ltd. *J. Am. Soc. Mass Spectrom.* **2007**, *18*, 1345–1346.

(13) Ure, M.; Thomas, R.; Littlejohn, D. Ammonium Acetate Extracts and Their Analysis for the Speciation of Metal Ions in Soils and Sediments. *Int. J. Environ. Anal. Chem.* **2006**, *51*, 65–84.

(14) van Leeuwen, H. P.; Town, R. M.; Buffle, J.; Cleven, R. F.; Davison, W.; Puy, J.; van Riemsdijk, W. H.; Sigg, L. Dynamic Speciation Analysis and Bioavailability of Metals in Aquatic Systems. *Environ. Sci. Technol.* **2005**, *39*, 8545–8556.

(15) Muñoz, J.; Gallego, M.; Valcárcel, M. Speciation analysis of mercury and tin compounds in water and sediments by gas chromatography-mass spectrometry following preconcentration on C60 fullerene. *Anal. Chim. Acta* **2005**, *548*, 66–72.

(16) Plavšií, M.; Cosovic, B. Influence of surface-active substances on the redox processes of metal ions: a contribution to the speciation analysis of metals in aquatic systems. *Anal. Chim. Acta* **1994**, *284*, 539–545.

(17) Sener, G.; Uzun, L.; Denizli, A. Lysine-promoted colorimetric response of gold nanoparticles: a simple assay for ultrasensitive mercury(II) detection. *Anal. Chem.* **2014**, *86*, 514–520.

(18) Dubois, M.; Gilles, K. A.; Hamilton, J. K.; Rebers, P. A.; Smith, F. Colorimetric Method for Determination of Sugars and Related Substances. *Anal. Chem.* **1956**, *28*, 350–356.

(19) Erel, O. A new automated colorimetric method for measuring total oxidant status. *Clin. Biochem.* **2005**, *38*, 1103–1111.

(20) Tian, X.; Chen, L.; Li, Y.; Yang, C.; Nie, Y.; Zhou, C.; Wang, Y. Design and synthesis of a molecule with aggregation-induced emission effects and its application in the detection of arsenite in groundwater. *J. Mater. Chem. C* **2017**, *5*, 3669–3672.

(21) Yetisen, A. K.; Montelongo, Y.; Qasim, M. M.; Butt, H.; Wilkinson, T. D.; Monteiro, M. J.; Yun, S. H. Photonic Nanosensor for Colorimetric Detection of Metal Ions. *Anal. Chem.* **2015**, *87*, 5101–5108.

(22) Awual, M. R.; Hasan, M. M. Colorimetric detection and removal of copper(II) ions from wastewater samples using tailor-made composite adsorbent. *Sens. Actuators, B* **2015**, *206*, 692–700.

(23) Mcgifford, R. W.; Seen, A. J.; Haddad, P. R. Direct colorimetric detection of copper(II) ions in sampling using diffusive gradients in thin-films. *Anal. Chim. Acta* **2010**, *662*, 44–50.

(24) Raja, S.; Gabriel, G. J.; Smith, C. E.; Aamer, K. A.; Tew, G. N. A highly selective colorimetric aqueous sensor for mercury. *Chem. - Eur. J.* **2010**, *14*, 3904–3907.

(25) Sharma, H.; Singh, A.; Kaur, N.; Singh, N. ZnO-Based Imine-Linked Coupled Biocompatible Chemosensor for Nanomolar Detection of Co^{2+}. *ACS Sustainable Chem. Eng.* **2013**, *1*, 1600–1608.

(26) Ondigo, D. A.; Tshentu, Z. R.; Torto, N. Electrospun nanofiber based colorimetric probe for rapid detection of Fe^{2+} in water. *Anal. Chim. Acta* **2013**, *804*, 228–234.

(27) Wang, Y.; Hu, J.; Zhuang, Q.; Ni, Y. Enhancing sensitivity and selectivity in a label-free colorimetric sensor for detection of iron(II) ions with luminescent molybdenum disulfide nanosheet-based peroxidase mimetics. *Biosens. Bioelectron.* **2016**, *80*, 111–117.

(28) Kuntz, I. D.; Gasparro, F. P.; Johnston, M. D.; Taylor, R. P. Molecular interactions and the Benesi-Hildebrand Equation. *J. Am. Chem. Soc.* **1968**, *90*, 4478–4481.

(29) Xu, Y.; Panzner, M. J.; Li, X.; Youngs, W. J.; Pang, Y. Host-guest assembly of squaraine dye in cucurbit[8]uril: its implication in fluorescent probe for mercury ions. *Chem. Commun.* **2010**, *46*, 4073–4075.

(30) Chen, L.; Tian, X.; Yang, C.; Li, Y.; Zhou, Z.; Wang, Y.; Xiang, F. Highly selective and sensitive determination of copper ion based on a visual fluorescence method. *Sens. Actuators, B* **2017**, *240*, 66–75.

(31) Dunning, T. H., Jr. Gaussian basis sets for use in correlated molecular calculations. I. The atoms boron through neon and hydrogen. *J. Chem. Phys.* **1989**, *90*, 1007–1023.

(32) Lu, T.; Chen, F. Multiwfn: A multifunctional wavefunction analyzer. *J. Comput. Chem.* **2012**, *33*, 580–592.

DOI: 10.1021/acsomega.9b00312
ACS Omega 2019, 4, 5915–5922